Supporting Information

Seven et al. 10.1073/pnas.1310327110

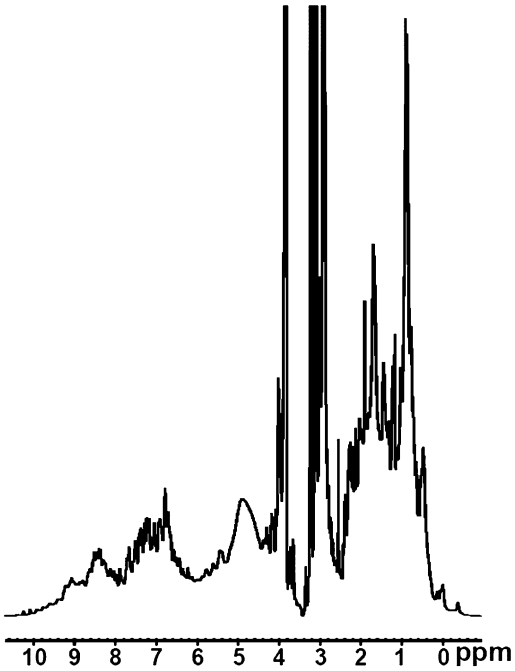

Fig. S1. ^{1}H NMR spectrum of 800 μM ^{15}*N*-C_2AB in 50 mM Mes (pH 6.3) containing 150 mM NaCl and 100 mM Ca^{2+}.

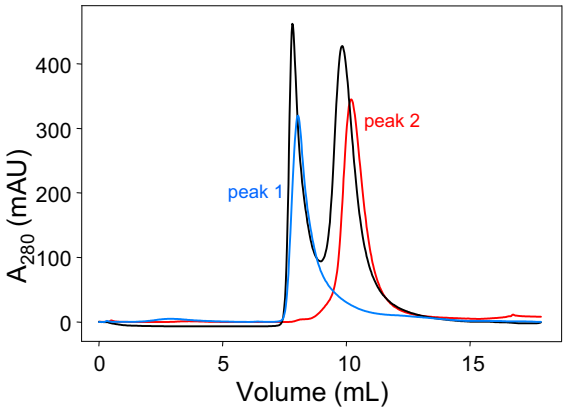

Fig. S2. Peaks 1 and 2 in the gel filtration profile of Fig. 3*A* correspond to stable species. The black curve shows the gel filtration profile on an analytical Superdex 75 10/300 column of an InC_2AB sample that was purified by our usual procedure, including the benzonase treatment, but without ion exchange chromatography step. A portion of the same sample was injected into a preparative Superdex 75 16/60 column; the fractions corresponding to peaks 1 and 2 were collected and then injected into the analytical Superdex 75 10/300 column (blue and red curves, respectively).

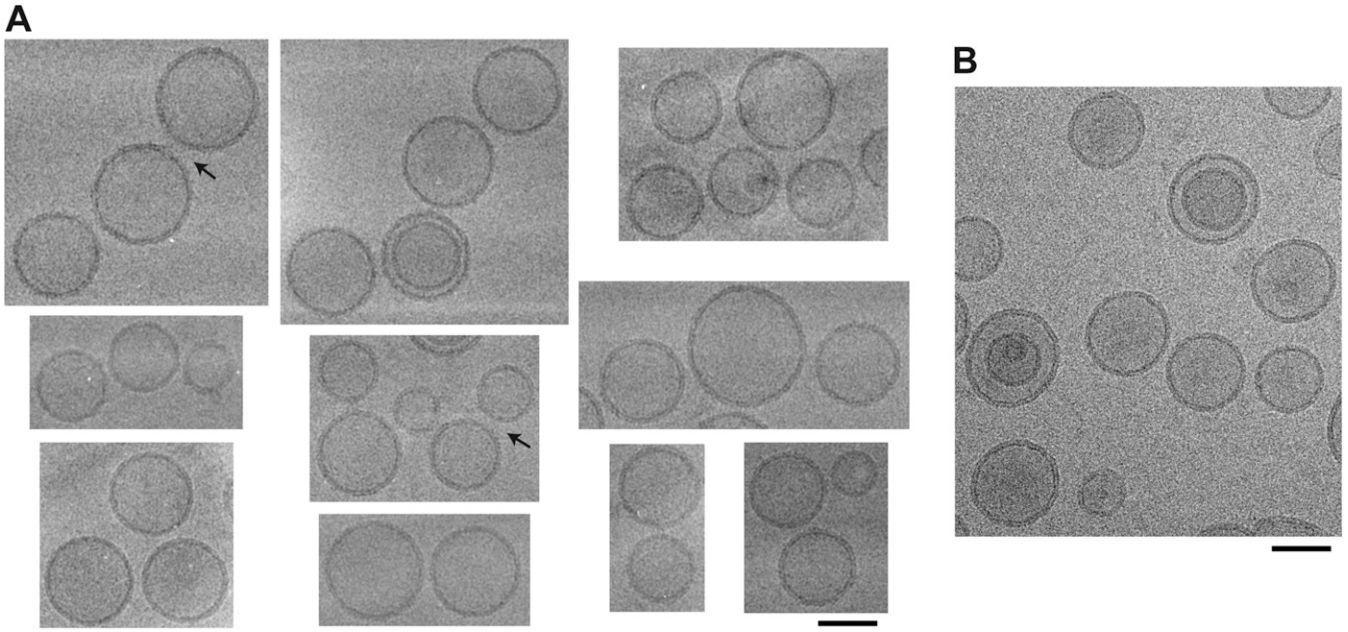

Fig. S3. Cryo-EM analysis of liposome clustering by lnC_2AB. Additional images of the same experiments described in Fig. 4. (*A*) The arrows point to interfaces with intermembrane distances of 8–10 nm and what appears to be electron density between them that could correspond to lnC_2AB oligomers. (*B*) Example of loosely clustered vesicles. (Scale bars: 100 nm.)

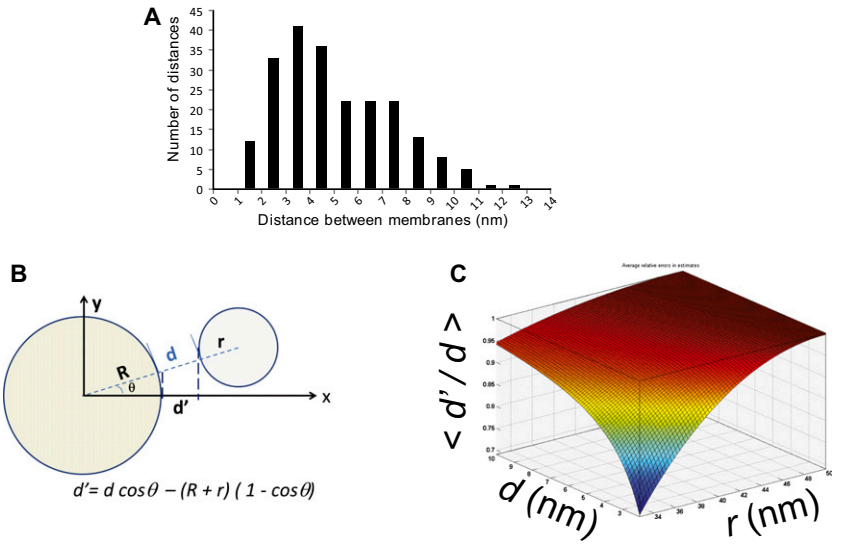

Fig. S4. Slight underestimation of intermembrane distance due to cryo-EM projection. (*A*) Histogram of intermembrane distances between vesicle pairs where both vesicles have diameters larger than 70 nm. The data correspond to a subpopulation of the whole set shown in Fig. 4*B*. (*B*) Geometrical considerations for two vesicles with intermembrane distance ***d*** positioned in different vertical planes. The two vesicles have different diameters, ***R*** and ***r***. The projection (along the *y* axis) gives an underestimated distance d'. (*C*) Average underestimation for the intermembrane distances between two vesicles. Without losing generality, here we assume that the diameter of the large vesicle is 100 nm, and the small vesicles vary from 65 to 100 nm in diameter. The thickness of the vitrified ice confined the possible displacement between these two vesicles. Because the big vesicles are close to the thickness of ice (≤100 nm), they are positioned with the origin in the center of the ice. The small vesicles are assumed to take a random vertical position (***y***) with an even probability, $p(y) = 1/(2R - 2r)$. The angle **θ** (defined in *B*) is estimated by

$$\sin\theta = \frac{y}{(R+r+d)}.$$

The average of d' is then calculated by estimating the average of cos θ.

$$\langle\cos\theta\rangle = \int_y SQRT(1-\sin\theta * \sin[(\theta) * p(y)dy)],$$

and the estimated average of d'/d becomes

$$\left\langle\frac{d'}{d}\right\rangle = \langle\cos\theta\rangle - \frac{R+r}{d}(1-\langle\cos\theta\rangle).$$

We did numerical calculations of the average d'/d, plotted them as a function of the intermembrane distance ***d*** (from 2 to 10 nm) and the radius of the small vesicles **r** (from 32 to 50 nm), and presented the results in a 3D surface plot. All of the simulations were done in MATLAB 11a (licensed through University of Texas Southwestern).

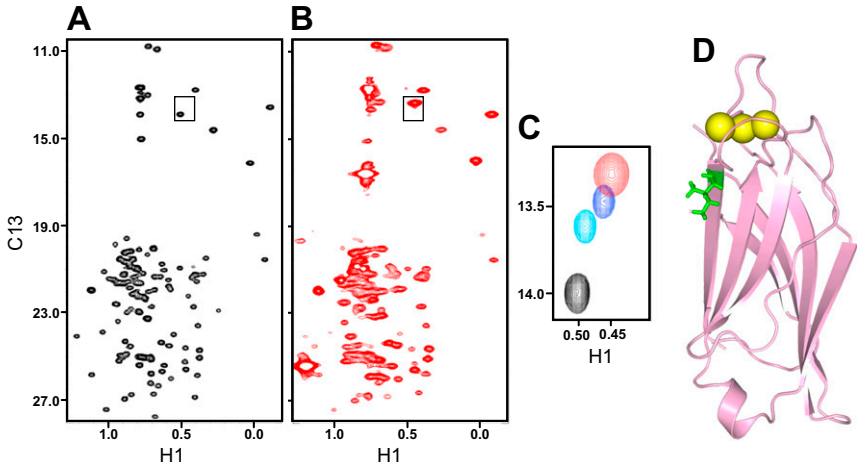

Fig. S5. NMR analysis of C_2AB on nanodiscs. (*A* and *B*) ^{1}H-^{13}C heteronuclear multiple-quantum coherence (HMQC) spectrum of 50 μM ^{2}H-ILV-$^{13}CH_3$-C_2AB in 1 mM EDTA (*A*) or in 1 mM Ca^{2+} in the presence of 60 μM nanodiscs (*B*). (*C*) Superposition of expansions showing the cross-peak from Ile239 (rectangle shown in *A* and *B*) of ^{1}H-^{13}C HMQC spectra of 50 μM ^{2}H-ILV-$^{13}CH_3$-C_2AB in 1 mM EDTA (black), 1 mM Ca^{2+} (cyan), 20 mM Ca^{2+} (blue), or 1 mM Ca^{2+} plus 60-μM nanodiscs (red). (*D*) Ribbon diagram of the synaptotagmin-1 C_2A showing the location of I239 as a green stick model. Ca^{2+} ions are shown as yellow spheres.

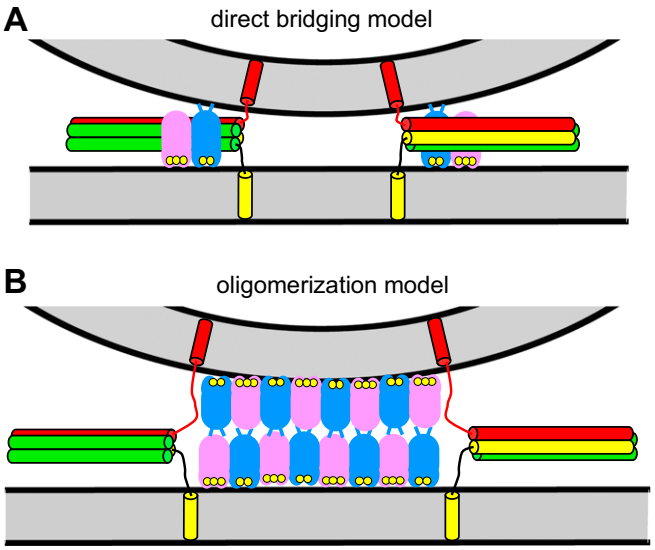

Fig. S6. Mechanistic implications of the direct bridging and oligomerization models. Both diagrams show the soluble N-ethylmaleimide sensitive factor adaptor protein receptor (SNARE) complex (syntaxin-1 in yellow, SNAP-25 in green, and synaptobrevin in red) bridging the synaptic vesicle and plasma membranes (shown in gray), and are intended to illustrate potential relative orientations of the synaptotagmin-1 C_2 domains (C_2A domain in pink, C_2B domain in blue, Ca^{2+} ions in yellow) with respect to the membranes and the SNARE complex. (*A*) In the direct bridging model, synaptotagmin-1 could bind simultaneously to the SNARE complex and the two membranes, which would allow a natural cooperation between synaptotagmin-1 and the SNAREs in bringing the membranes together to induce membrane fusion (1, 2). (*B*) In the oligomerization model, formation of a single synaptotagmin-1 oligomer between the membranes would hinder membrane fusion. It could be envisaged that multiple synaptotagmin-1 oligomers could form around the fusion pore area and each oligomer could bind to a SNARE complex, but neurotransmitter release is believed to normally involve a minimum of three SNARE complexes (3), and therefore this model would require an unrealistic number of synaptotagmin-1 molecules. Note that the transmembrane region of synaptotagmin-1 and the linker from this region to the C_2A domain are not shown for simplicity. Because this linker spans more than 50 residues and is highly flexible, it is expected to allow a very wide range of orientations of the C_2 domains with respect to the two membranes.

1. Araç D, et al. (2006) Close membrane-membrane proximity induced by Ca(2+)-dependent multivalent binding of synaptotagmin-1 to phospholipids. *Nat Struct Mol Biol* 13(3):209–217.
2. Dai H, Shen N, Araç D, Rizo J (2007) A quaternary SNARE-synaptotagmin-Ca2+-phospholipid complex in neurotransmitter release. *J Mol Biol* 367(3):848–863.
3. Mohrmann R, de Wit H, Verhage M, Neher E, Sørensen JB (2010) Fast vesicle fusion in living cells requires at least three SNARE complexes. *Science* 330(6003):502–505.